Supporting Information

Nanoscale Selective Passivation of Electrodes Contacting a 2D Semiconductor

Martina Lihter, Michael Graf, Damir Iveković and Aleksandra Radenovic**

M. Lihter, Dr. M. Graf, Prof. A. Radenovic
Laboratory of Nanoscale Biology, Institute of Bioengineering, School of Engineering, EPFL, Lausanne, 1015, Switzerland
E-mail: martina.lihter@epfl.ch, aleksandra.radenovic@epfl.ch

Prof. D. Iveković
Laboratory of General and Inorganic Chemistry and Electroanalysis, Faculty of Food Technology and Biotechnology, University of Zagreb, Zagreb, 10 000, Croatia

Table of Contents

1. Thin-film Deposition Techniques

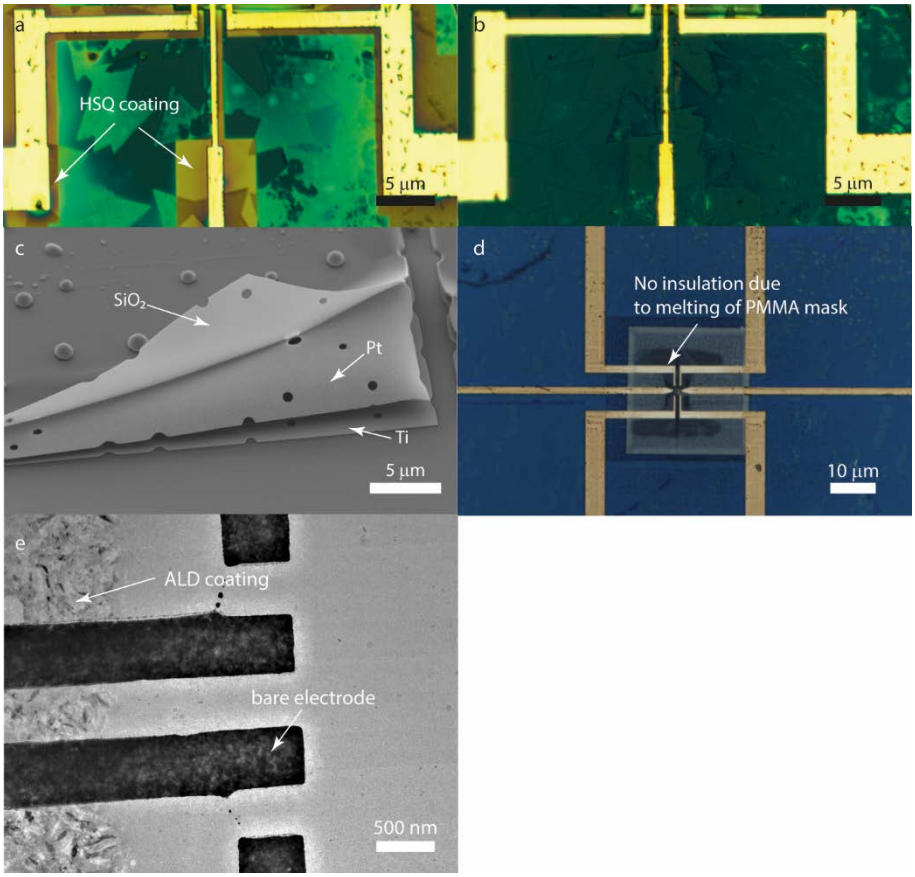

Figure S1. Challenges in thin-film deposition techniques (a) An optical image of the electrodes coated with hydrogen silsesquioxane (HSQ) before and after (b) the exposure to 0.1 M KCl solution. Due to its porosity, the layer completely dissolves after exposing to the solution. (c) An SEM image showing the delamination of the evaporated SiO_2 layer covering Ti / Pt electrodes due to the poor adhesion to underlying layer. The holes in the layers occur due to micron-sized resist residues that were not completely removed before the deposition. (d) An optical micrograph of the metal contacts after the ALD deposition. The contrast increase on the electrode and their vicinity shows the absence of the insulation layer. At high temperatures required for ALD deposition, the PMMA photoresist mask starts reflowing, which destroys the pattern and prevents the ALD coating from depositing at the electrodes. (e) A TEM image of the electrodes of another device passivated by the same method as in (d).

2. Poly(phenylene oxide) Deposition

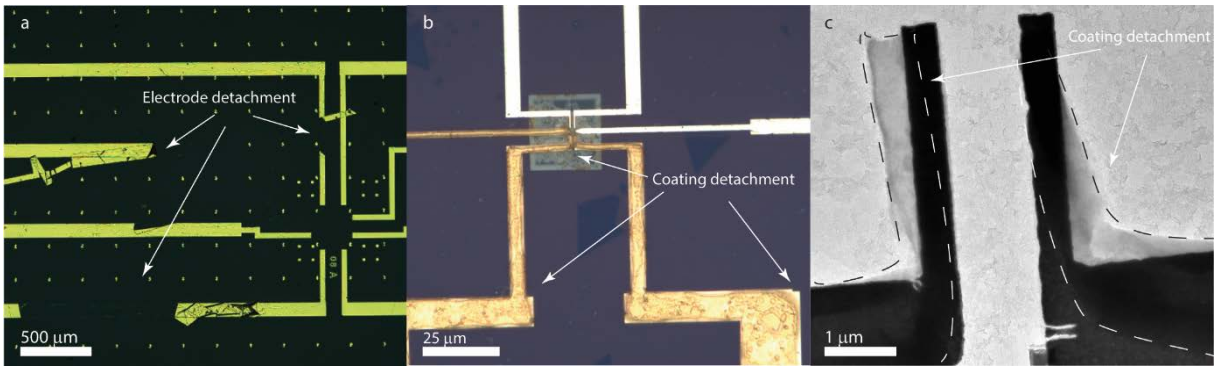

Figure S2. Challenges during PPO thin-film deposition. (a) An optical micrograph of detached Cr / Pt electrodes due to electrode oxidation during voltage cyclization in a water-based solution. An optical micrograph (b) and a TEM micrograph (c) showing the detached PPO coating after heating to approx. 100°C, which occurs due to the difference in the thermal expansion between the metal and the PPO polymer. This is pronounced in the case of electrodes with a high aspect ratio, especially at the micro- and nanoscale.

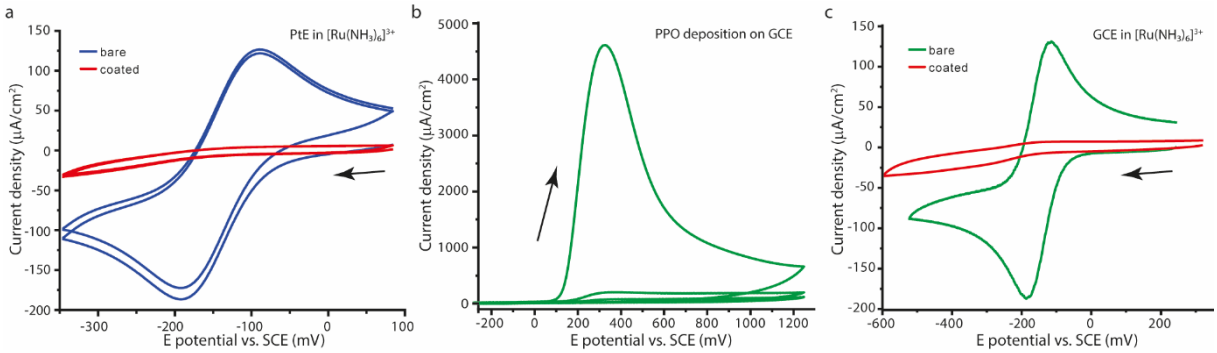

Figure S3. Cyclic voltammograms on macroscopic electrodes. (**a**) Cyclic voltammograms of PtE before and after PPO deposition in 1mM $[Ru(NH_3)_6]^{3+}$ with 0.1 M KNO_3 as a supporting electrolyte. (**b**) PPO deposition on glassy carbon electrode (GCE). The deposition was performed during 10 cycles in a solution of 50 mM phenol, 50 mM TMAH*5H_2O and 0.1 M TBAP in acetonitrile. (**c**) Cyclic voltammograms obtained on GCE, before and after the PPO deposition, in 1mM $[Ru(NH_3)_6]^{3+}$ with 0.1 M KNO_3 as a supporting electrolyte. All measurements were done with a scan rate of 50 mV s^{-1}. The arrows indicate the scan direction.

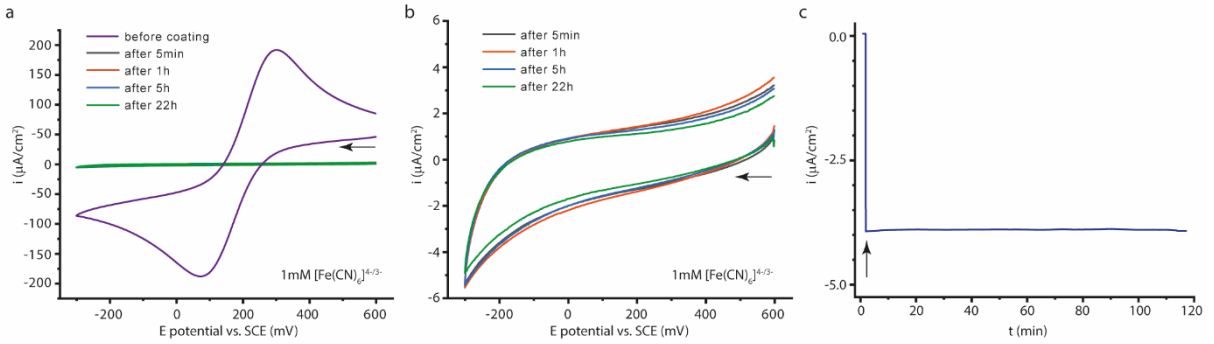

Figure S4. Coating stability. (**a**) Cyclic voltammograms of GCE before and after coating in 1 mM $[Fe(CN)_6]^{4-/3-}$ and 0.1 M KNO_3 as a supporting electrolyte. The electrode was continuously exposed to the solution for 22 h, while the measurements were taken after 5 min, 1 h, 5 h and 22 h. All measurements were done with a scan rate of 50 mV s^{-1}. The arrow indicates the scan direction. (**b**) Close-up view of CV measurements in (**a**). (**c**) Platinum rotating disc electrode coated with PPO was initially held at the rest potential in solution of 1 mM $[Fe(CN)_6]^{4-/3-}$ with 0.1 M KNO_3 as a supporting electrolyte. At t =1 min (as indicated by arrow) the electrode was polarized to -100 mV vs. SCE and was held at that potential for the next two hours. No change in the ferricyanide reduction current was observed. The experiment was performed under hydrodynamic conditions with an electrode rotation rate of 600 rpm.

3. X-ray Photoelectron Spectroscopy

We recorded a survey spectrum and high-resolution spectra regions (Figure S5) of PPO film deposited on a Pt substrate. The Pt signal is very low which shows almost complete surface coverage with PPO. The Pt 4f, C 1s, and O 1s signals were fitted and assigned to different chemical environments according to the references given in Table S1. From the area of the Pt 4f signal, we estimated that the O 1s signal originating from PtO / PtO_2 constitutes less than 1% of the total O 1s signal. Therefore, the O 1s signal that originates from PtO / PtO_2 was not fitted. The ratio of the O 1s peak areas, which is 16767 / 4259 = 3.9 : 1, indicates that on approximately four -O-Ph-O- units there is one Ph – OH unit (*Ph*- = phenyl group). Table S2 reports the atomic concentration of elements present in the layer.

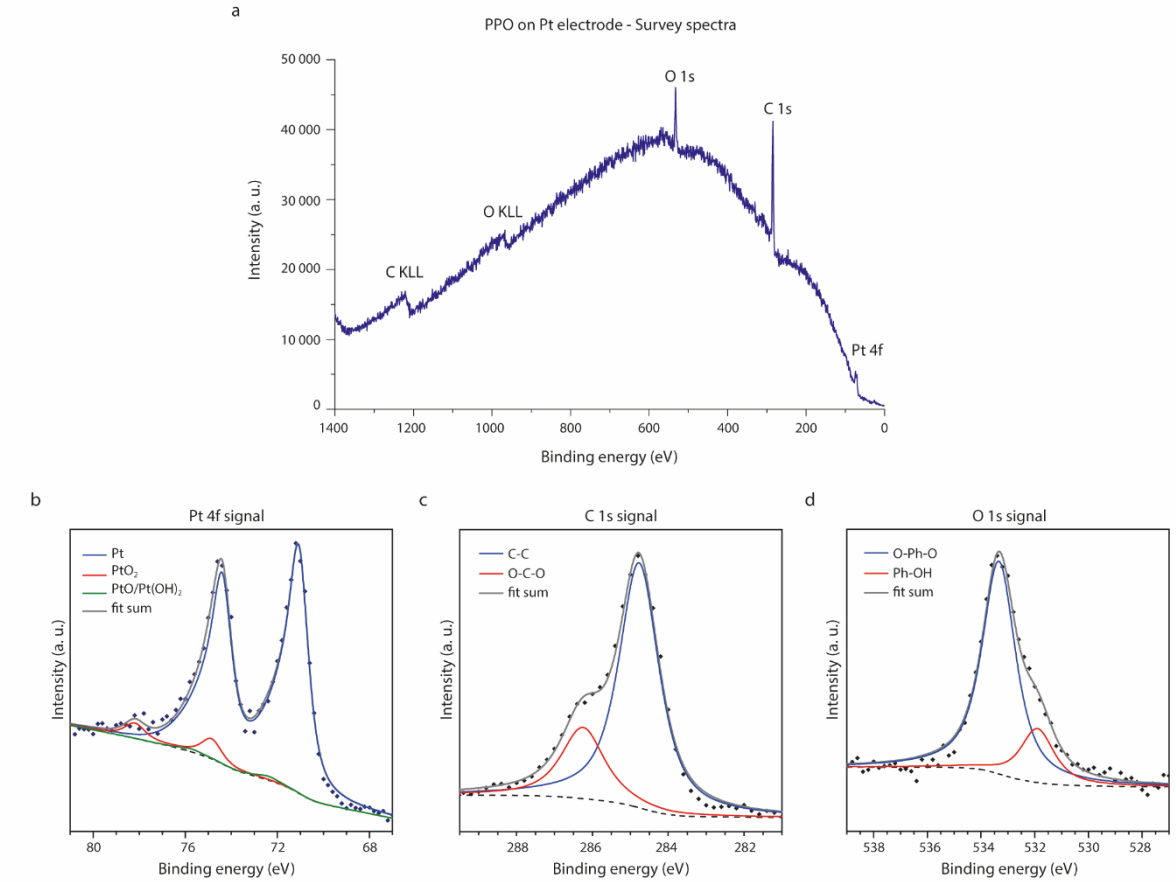

Figure S5. XPS analysis of PPO film deposited on Pt electrode. (a) Survey spectra. (b-d) High-resolution spectra regions and Pt 4f, C 1s, O 1s signal fitting.

Table S1. XPS signals assigned to different peaks. "Ph-" = phenyl group

Signal	Binding energies / eV	FWHM	Peak area	Chemical state	Reference
Pt 4f	71.1	0.95	10556	Pt	[1]
	74.9	1.0	588	PtO_2	[2]
	72.4	1.0	116	$PtO/Pt(OH)_2$	[2]
C 1s	284.8	1.22	32359	C-C	[3]
	286.2	1.30	10060	O-C-O	[3]
O 1s	533.3	1.44	16767	O-Ph-O	[3]
	531.9	1.44	4259	Ph-O	[4]

Table S2. Atomic concentration table of PPO coating layer deposited on Pt electrode.

	C 1s	N 1s	O 1s	F 1s	Cl 2p	Pt 4f
at%	82.21	1.48	15.47	0.01	0.00	0.82

4. Scanning Electron Microscopy

The smoothness of PPO coating was inspected in scanning electron microscopy (SEM) on Pt substrates (Figure S6a and b). At an acceleration voltage of 3 kV, the thin PPO film is transparent to electrons, therefore, the images mostly reveal the morphology of the Pt. By using the graphite flakes as the substrates (Figure S6c) and limiting the acceleration voltages to below 1 kV, we managed to collect more information from the PPO surface (Figure S6d). Although the signal from the underlying Pt is still present, PPO film shows very smooth and homogeneous coatings at the measured scales.

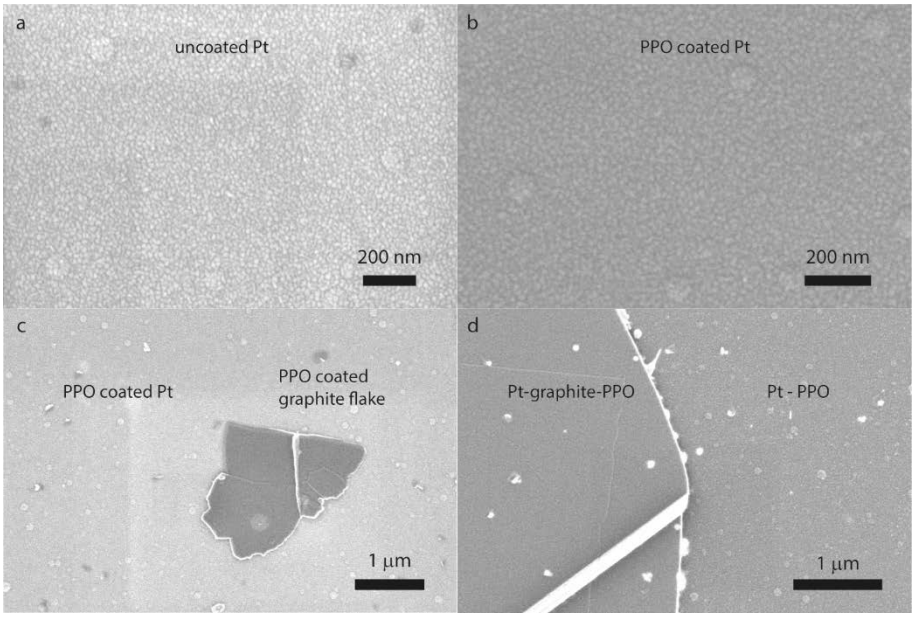

Figure S6. SEM micrographs. (a) A bare Pt substrate (imaging conditions: 3 kV). (b) Pt coated with PPO (3 kV). Circular features (d~100 nm) originate from defective Pt surface and can be seen in (a). (c) An example of a PPO coated graphite flake on a Pt substrate (1 kV). (d) The comparison of PPO coating on graphite flake vs. PPO on the Pt surface (500 V).

5. Atomic Force Microscopy

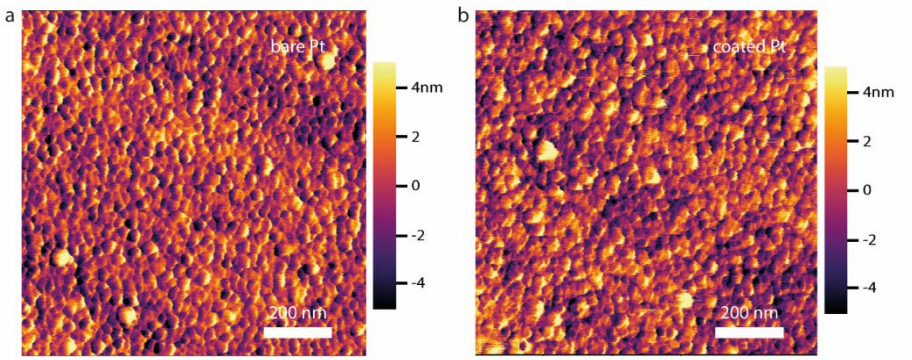

Figure S7. AFM micrographs of Pt substrate before (a) and after the deposition of approx. 10 nm thin PPO film (b). Due to the relatively high roughness of the bare Pt electrode surface (S_{dev}=2.201 nm, A_{dev}=1.715 nm), the difference in surface roughness before and after the deposition (S_{dev}=2.202 nm, A_{dev}=1.693 nm) is not visible. The micrograph is not taken from the same area. S_{dev} , standard deviation; A_{dev} , average deviation.

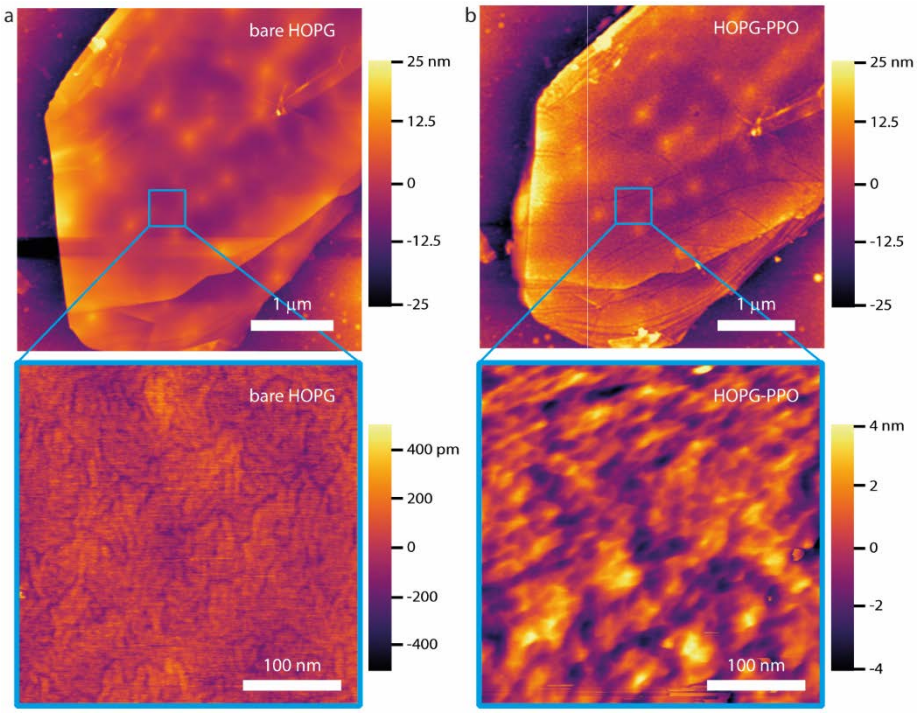

Figure S8. AFM micrographs of PPO coating on HOPG. A HOPG crystal before (a) and after PPO coating (b). Close-up views show the same 350 x 350 nm^2 region before and after the coating.

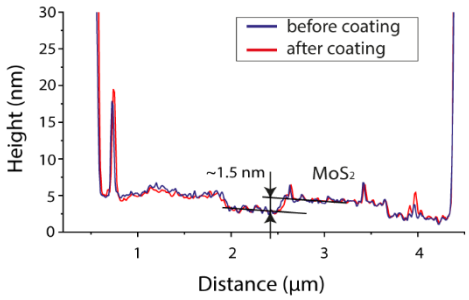

Figure S9. The AFM cross-section of MoS_2 layer before (blue) and after (red) coating the electrodes with PPO. The MoS_2 height stays unchanged which indicates that the PPO deposition did not occur on the MoS_2.

6. Conductance Measurements

Before coating the electrodes with PPO, the conductance of the MoS_2 was measured at room-temperature in air, and in vacuum after the annealing process, respectively. The conductance increase several orders of magnitude in vacuum confirming that the devices are operational. After exposure to air, the conductance drops again to the initial values.

During the coating process the electrodes of the devices 3, 6, 8 and 9 were coated with PPO film while the others were kept as a control by being exposed to the same solution without coating. The data are represented in Table S3, and graphically in Figure S10. The enhanced conductance in some devices after the deposition might originate from reversible physisorption of aromatic molecules which is consistent with the results reported by Wang et al.[5]

Table S3. The conductance, G, of MoS_2 devices before and after the PPO coating.

	Before PPO deposition		After PPO deposition
Device	Initial G / pS	In vacuum G / pS	G / pS
1	4.9	4460	667
2	6.3	11100	111
3	4.8	9900	131
4	11	24100	8
5	36.6	58400	11
6	13.1	21200	223
7	37.7	61200	16
8	7.4	85200	3.7
9	6.5	26000	5.5

All measurements were done in a two-terminal configuration, at RT and in air, except the ones done in a vacuum (base pressure 10^{-6} mbar) after the annealing treatment. The electrodes of the devices marked in red were coated with PPO, while the others were kept as a control exposing them to a coating solution during the deposition.

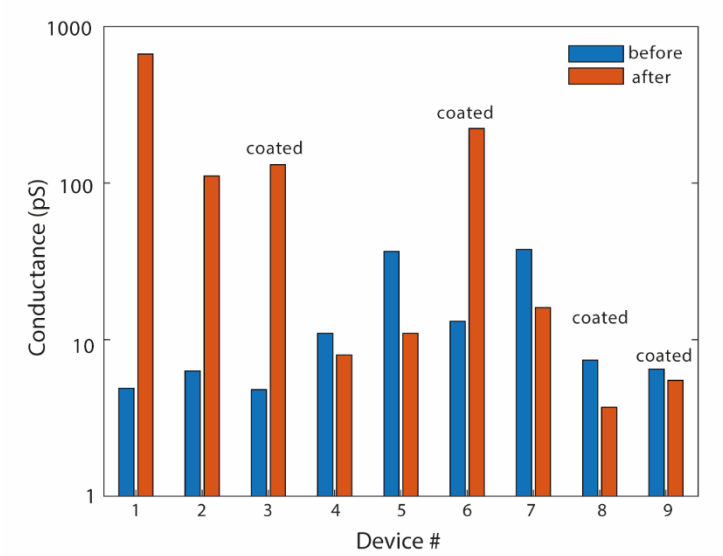

Figure S10. A graphical representation of the device's conductance in air before and after the PPO coating process.

7. Number of Devices

Suspended MoS_2 devices (Nanopore-FET): In total, we have tested approx. 30 contacted MoS_2 nanoribbons. 12 of them were used during the process optimization (#cycles, voltage range), 8 of them were used with the final parameters presented in this manuscript, and 10 were kept as a control. 15 ribbons were checked in TEM before and after the coating. In all cases, MoS_2 stayed uncoated.

Supported MoS_2 devices: In total, we fabricated 24 pairs of electrodes, each contacting one MoS_2 triangle. 40% of them were checked by AFM. Again, in all cases MoS_2 stayed uncoated.

8. References

[1] J. S. Hammond, N. Winograd, *J. Electroanal. Chem.* 1977, *78*, 55.
[2] J. L. G. Fierro, J. M. Palacios, F. Tomas, *Surf. Interface Anal.* 1988, *13*, 25.
[3] M. C. Burrell, J. J. Chera, *Surf. Sci. Spectra* 2002, *6*, 9.
[4] B. Folkesson, P. Sundberg, *Spectrosc. Lett.* 1987, *20*, 193.
[5] Y. Wang, A. Slassi, M. Stoeckel, S. Bertolazzi, J. Cornil, D. Beljonne, P. Samorì, *J. Phys. Chem. Lett.* 2019, *10*, 540.